LBL-32342
UC-413
Preprint

Lawrence Berkeley Laboratory
UNIVERSITY OF CALIFORNIA

Submitted to Physical Review C

Relativistic Thomas-Fermi Calculations of Hot Nuclei

D. Von-Eiff and M.K. Weigel

May 1992

| LOAN COPY |
|Circulates |
|for 4 weeks| Bldg. 50 Library.
Copy 2
LBL-32342

Prepared for the U.S. Department of Energy under Contract Number DE-AC03-76SF00098

DISCLAIMER

This document was prepared as an account of work sponsored by the United States Government. Neither the United States Government nor any agency thereof, nor The Regents of the University of California, nor any of their employees, makes any warranty, express or implied, or assumes any legal liability or responsibility for the accuracy, completeness, or usefulness of any information, apparatus, product, or process disclosed, or represents that its use would not infringe privately owned rights. Reference herein to any specific commercial product, process, or service by its trade name, trademark, manufacturer, or otherwise, does not necessarily constitute or imply its endorsement, recommendation, or favoring by the United States Government or any agency thereof, or The Regents of the University of California. The views and opinions of authors expressed herein do not necessarily state or reflect those of the United States Government or any agency thereof or The Regents of the University of California and shall not be used for advertising or product endorsement purposes.

Lawrence Berkeley Laboratory is an equal opportunity employer.

DISCLAIMER

This document was prepared as an account of work sponsored by the United States Government. While this document is believed to contain correct information, neither the United States Government nor any agency thereof, nor the Regents of the University of California, nor any of their employees, makes any warranty, express or implied, or assumes any legal responsibility for the accuracy, completeness, or usefulness of any information, apparatus, product, or process disclosed, or represents that its use would not infringe privately owned rights. Reference herein to any specific commercial product, process, or service by its trade name, trademark, manufacturer, or otherwise, does not necessarily constitute or imply its endorsement, recommendation, or favoring by the United States Government or any agency thereof, or the Regents of the University of California. The views and opinions of authors expressed herein do not necessarily state or reflect those of the United States Government or any agency thereof or the Regents of the University of California.

LBL–32342

Relativistic Thomas–Fermi Calculations of Hot Nuclei *

D. Von-Eiff † and M.K. Weigel ‡

May 15, 1992

Nuclear Science Division
Lawrence Berkeley Laboratory
University of California
Berkeley, California 94720, U.S.A.

Abstract

Relativistic thermal Thomas–Fermi calculations for equilibrated hot nuclei have been performed for a non–linear σ–ω model. To isolate the properties of the hot nucleus from the contributions of the surrounding nucleon vapor, a subtraction procedure based on the "equivalent sharp radius" is applied. Various quantities describing hot nuclei and their temperature dependence are investigated. Special attention is devoted to the study of the level density parameter; we compare our results with those of a recently published nonrelativistic investigation.

PACS numbers: 05.30.Fk, 21.10.Dr, 21.10.Ma

*This work was supported by the Director, Office of Energy Research, Office of High Energy and Nuclear Physics, Division of Nuclear Physics, of the U.S. Department of Energy under Contract DE–AC03–76SF00098, and the Deutscher Akademischer Austauschdienst (DAAD).

†DAAD fellow. Permanent address: Sektion Physik der Ludwig–Maximilians–Universität München, Theresienstraße 37/III, W–8000 München 2, Bundesrepublik Deutschland.

‡Sektion Physik der Ludwig–Maximilians–Universität München, Am Coulombwall 1, W–8046 Garching, Bundesrepublik Deutschland

1 Introduction

In the last decade two elements have strongly influenced the description of nuclear systems. First there has been growing interest in describing nuclear systems within a relativistic framework. One of the most popular models is the relativistic mean field theory by Walecka (for a review, see Ref. [1]). It is a phenomenological approach including nucleonic and mesonic degrees of freedom, in which the coupling constants and some meson masses are taken as free parameters and are adjusted to fit the properties of nuclear matter and finite nuclei. In the original Walecka model the incompressibility of nuclear matter is considerably too large. Therefore Boguta and Bodmer [2] included two additional free parameters through cubic and quartic terms in the scalar field which shift the incompressibility to more reasonable values in comparison with the experimental data. In addition, one obtains the freedom to fix the value of the nuclear matter effective mass M^* which, for fixed saturation density and binding energy, determines completely the energy dependence of the optical potential. The nonlinear σ–ω model has been widely and successfully used in nuclear matter and finite nuclei calculations (see, for instance, Refs. [3, 4]) to describe ground state properties.

Second the use of "temperature" in the description of excited systems has obtained a growing importance. In the relativistic scheme several authors have used quantum statistical methods for infinite systems [1, 5–11], since one is strongly interested in the equation of state, which is of great importance for astrophysical problems. For finite systems various authors have investigated the thermal properties of hot nuclei within nonrelativistic models [12–18] because heavy ion collisions at intermediate bombarding energies (10–100 MeV/A) give strong experimental evidence for the formation of highly excited nuclei [19].

In a recent paper we developed a relativistic thermal Hartree–Fock model and its semiclassical approximation [20]. The purpose of this paper is to present relativistic thermal Thomas–Fermi calculations of hot nuclei; i.e. calculations within a semiclassical approximation of the Hartree part of the model in Ref. [20], neglecting exchange terms. To our knowledge, so far one has not tried such kind of calculations. *Thomas–Fermi* approximation means to assume that the meson fields vary slowly enough in space so that the nucleons can be treated as moving in locally constant fields at each point. This approximation becomes more and more valid with increasing temper-

ature because the spatial dependence of the meson fields smooths out. In addition shell effects are vanishing at higher temperatures. Suraud [15] compared in the nonrelativistic scheme in detail semiclassical results with the Hartree–Fock calculations of Bonche et.al. [12, 13] and found good agreement for "high" temperatures (T>3 MeV). Moreover, at "low" temperatures (T$\leq$3 MeV), when shell effects are still present, the average quantal values were found to be correctly reproduced within the semiclassical framework. These integrated/average physical properties such as the excitation energy and the entropy are the quantities we are mostly interested in. In addition, the general advantage of semiclassical approaches which consists in the avoidance of numerically involved wave function calculations, holds in particular in the thermal case, because the number of states accessible to the hot nucleus increases as an exponential of the temperature [21]. Therefore it seems worthwhile to investigate hot nuclei in the framework of a relativistic thermal Thomas–Fermi approximation which provides a relatively simple model along with a tractable numerical effort for the selfconsistent solution.

The paper is organized as follows: in section 2 we derive the relativistic thermal Thomas–Fermi approximation (RTTFA). The subtraction mechanism to obtain thermostatic properties of hot nuclei which are independent on the size of the box in which the calculations are performed is described in section 3. Section 4 is devoted to the presentation of the results. In particular we discuss the thermostatic properties of ^{208}Pb. Special attention is paid to the level density parameter; we compare our results with those of a recent paper by de Lima Medeiros and Randrup [18], who used a nonrelativistic modified Seyler–Blanchard potential. In section 5 we give our main conclusions.

2 The relativistic thermal Thomas–Fermi approximation (RTTFA)

We want to investigate nuclear systems whose dynamics are governed by the following extended Walecka–Lagrangian [1]:

$$\mathcal{L} = \mathcal{L}_N^0 + \sum_{M=\sigma,\omega,\varrho,A} \left[\mathcal{L}_M^0 + \mathcal{L}_{MN}\right] + \mathcal{L}_{\sigma_{NL}} \tag{2.1}$$

with the free nucleon– and meson–Lagrangians

$$\begin{aligned}
\mathcal{L}_N^0(x) &= \bar{\psi}(x)\left(i\gamma_\mu\partial^\mu - M\right)\psi(x), && (2.2)\\
\mathcal{L}_\sigma^0(x) &= \frac{1}{2}\left(\partial_\mu\varphi(x)\partial^\mu\varphi(x) - m_\sigma^2\varphi^2(x)\right), && (2.3)\\
\mathcal{L}_\omega^0(x) &= \frac{1}{2}m_\omega^2\omega_\mu(x)\omega^\mu(x) - \frac{1}{4}F_{\mu\nu}(x)F^{\mu\nu}(x), && (2.4)\\
\mathcal{L}_\varrho^0(x) &= \frac{1}{2}m_\varrho^2\vec{\varrho}_\mu(x)\vec{\varrho}^\mu(x) - \frac{1}{4}\vec{G}_{\mu\nu}(x)\vec{G}^{\mu\nu}(x) && (2.5)
\end{aligned}$$

and the free contribution of the electromagnetic field

$$\mathcal{L}_A^0(x) = -\frac{1}{4}A_{\mu\nu}(x)A^{\mu\nu}(x), \tag{2.6}$$

where the field tensors are given in the usual way:

$$\begin{aligned}
F_{\mu\nu}(x) &= \partial_\mu\omega_\nu(x) - \partial_\nu\omega_\mu(x), && (2.7)\\
A_{\mu\nu}(x) &= \partial_\mu A_\nu(x) - \partial_\nu A_\mu(x), && (2.8)\\
\vec{G}_{\mu\nu}(x) &= \partial_\mu\vec{\varrho}_\nu(x) - \partial_\nu\vec{\varrho}_\mu(x). && (2.9)
\end{aligned}$$

The interaction terms $\mathcal{L}_{MN}(x)$ are given by:

$$\begin{aligned}
\mathcal{L}_{\sigma N}(x) &= g_\sigma\bar{\psi}(x)\varphi(x)\psi(x), && (2.10)\\
\mathcal{L}_{\omega N}(x) &= -g_\omega\bar{\psi}(x)\gamma^\mu\omega_\mu(x)\psi(x), && (2.11)\\
\mathcal{L}_{\varrho N}(x) &= -g_\varrho\bar{\psi}(x)\gamma^\mu\vec{\tau}\vec{\varrho}_\mu(x)\psi(x), && (2.12)\\
\mathcal{L}_{AN}(x) &= -e\bar{\psi}(x)\gamma^\mu\frac{1+\tau_3}{2}A_\mu(x)\psi(x). && (2.13)
\end{aligned}$$

Nonlinear selfinteractions of the σ–meson are also taken into account [2]:

$$\mathcal{L}_{\sigma_{NL}}(x) = -\frac{1}{3}Mb\left(g_\sigma\varphi(x)\right)^3 - \frac{1}{4}c\left(g_\sigma\varphi(x)\right)^4. \tag{2.14}$$

With the assumption of spherical symmetry, charge conservation, a static approximation for the meson– and electromagnetic fields and replacing the meson– and electromagnetic field operators by their mean field values, a standard Legendre transformation yields:

$$
\begin{aligned}
\hat{H} = & \int_V d^3r \left\{ \hat{\bar{\psi}}(\vec{r}) \left(-i\vec{\gamma}\cdot\vec{\nabla} + M^*(r) \right) \hat{\psi}(\vec{r}) + \right. \\
& + \frac{1}{2} \left(\vec{\nabla}\varphi(r) \right)^2 + U\left[\varphi(r)\right] - \\
& - \frac{1}{2} \left[\left(\vec{\nabla}\omega_0(r) \right)^2 + m_\omega^2 \omega_0^2(r) \right] - \\
& - \frac{1}{2} \left[\left(\vec{\nabla}\varrho_{00}(r) \right)^2 + m_\varrho^2 \varrho_{00}^2(r) \right] - \\
& - \frac{1}{2} \left(\vec{\nabla} A_0(r) \right)^2 + \\
& \left. + g_\omega \omega_0(r) \hat{\psi}^\dagger(\vec{r}) \hat{\psi}(\vec{r}) + g_\varrho \varrho_{00}(r) \hat{\psi}^\dagger(\vec{r}) \tau_3 \hat{\psi}(\vec{r}) + e A_0(r) \hat{\psi}^\dagger(\vec{r}) \frac{1+\tau_3}{2} \hat{\psi}(\vec{r}) \right\}
\end{aligned}
\tag{2.15}
$$

with

$$
M^*(r) = M - g_\sigma \varphi(r), \tag{2.16}
$$

$$
U\left[\varphi(r)\right] = \frac{1}{2} m_\sigma^2 \varphi^2(r) + \frac{1}{3} M b \left(g_\sigma \varphi(r) \right)^3 + \frac{1}{4} c \left(g_\sigma \varphi(r) \right)^4 . \tag{2.17}
$$

In the following the indices of the $\omega-$, $\varrho-$ and electromagnetic field are dropped for simplicity.

A *Thomas–Fermi* approximation means that the nucleon field operators in (2.15) are expanded locally into plane waves:

$$
\hat{\psi}(\vec{r}) \propto \sum_{\vec{k},\lambda} \left[\hat{A}_{\vec{k},\lambda} U\left(r, \vec{k}, \lambda\right) e^{i\vec{k}\cdot\vec{r}} + \hat{B}^\dagger_{\vec{k},\lambda} V\left(r, \vec{k}, \lambda\right) e^{-i\vec{k}\cdot\vec{r}} \right] . \tag{2.18}
$$

Substitution of this field expansion into the Hamiltonian (2.15), use of orthonormality relations and normal ordering of the creation– and destruction operators yield a diagonal mean–field Hamiltonian $\hat{H}_{MFT}$.

To investigate a nuclear system at finite temperature, we calculate the grand potential Ω using the standard expressions from statistical mechanics:

$$
\Omega = -\frac{1}{\beta} \ln Z_G, \tag{2.19}
$$

with the grand partition function

$$Z_G = \mathrm{Tr}\, e^{-\beta\left(\hat{H}-\mu_p\hat{Z}-\mu_n\hat{N}\right)}, \tag{2.20}$$

and

$$\beta = \frac{1}{T} \tag{2.21}$$

(we use units with $\hbar = c = k_B = 1$). For $\hat{H}$ we insert the mean–field Hamiltonian, $\hat{Z}$ and $\hat{N}$ are the proton– and neutron number operators, respectively. We assume that there are no antinucleons in the nuclear system. In addition it is well known from nuclear matter calculations [6–11] that in the temperature region under consideration (T < 20 MeV) nucleon–antinucleon pair production does not occur. Therefore we can neglect all antinucleon contributions. As usual, the nucleon–nucleon interaction is described as in the ground–state T=0; i.e. no temperature dependence of the meson– and electromagnetic fields is included [10].

Using standard techniques [22] one gets:

$$\begin{aligned}
&\Omega\left(\mu, V, T; \varphi(r); \vec{\nabla}\varphi(r); \omega(r), \vec{\nabla}\omega(r); \varrho(r); \vec{\nabla}\varrho(r); A(r); \vec{\nabla}A(r)\right) = \\
&= \int\limits_V d^3r \Bigg\{ \frac{1}{2}\left(\vec{\nabla}\varphi(r)\right)^2 + U\left[\varphi(r)\right] - \\
&\quad -\frac{1}{2}\left(\left(\vec{\nabla}\omega(r)\right)^2 + m_\omega^2\omega^2(r)\right) - \\
&\quad -\frac{1}{2}\left(\left(\vec{\nabla}\varrho(r)\right)^2 + m_\varrho^2\varrho^2(r)\right) - \\
&\quad -\frac{1}{2}\left(\vec{\nabla}A(r)\right)^2 - \\
&\quad -\frac{1}{\beta\pi^2}\int\limits_0^\infty dp\, p^2 \ln\left(1 + e^{\beta\left(\mu_p - \sqrt{p^2+M^{*2}(r)} - g_\omega\omega(r) - g_\varrho\varrho(r) - eA(r)\right)}\right) - \\
&\quad -\frac{1}{\beta\pi^2}\int\limits_0^\infty dp\, p^2 \ln\left(1 + e^{\beta\left(\mu_n - \sqrt{p^2+M^{*2}(r)} - g_\omega\omega(r) + g_\varrho\varrho(r)\right)}\right)\Bigg\}.
\end{aligned} \tag{2.22}$$

In the final step one applies the variational principle to (2.22) and obtains:

$$\left(\Delta - m_\sigma^2\right)\varphi(r) \;=\; -g_\sigma\rho_S(r) + Mb\left(g_\sigma\varphi(r)\right)^2 + c\left(g_\sigma\varphi(r)\right)^3, \tag{2.23}$$

$$\left(\Delta - m_\omega^2\right)\omega(r) = -g_\omega \rho_B(r), \tag{2.24}$$

$$\left(\Delta - m_\varrho^2\right)\varrho(r) = -g_\varrho \rho_3(r), \tag{2.25}$$

$$\Delta A(r) = -e\rho_p(r), \tag{2.26}$$

with the densities

$$\rho_p(r) = \frac{1}{\pi^2}\int_0^\infty dp\, p^2 \frac{1}{\left(1 + e^{\beta\left(\sqrt{p^2+M^{*2}(r)}+g_\omega\omega(r)+g_\varrho\varrho(r)+eA(r)-\mu_p\right)}\right)}, \tag{2.27}$$

$$\rho_n(r) = \frac{1}{\pi^2}\int_0^\infty dp\, p^2 \frac{1}{\left(1 + e^{\beta\left(\sqrt{p^2+M^{*2}(r)}+g_\omega\omega(r)-g_\varrho\varrho(r)-\mu_n\right)}\right)}, \tag{2.28}$$

$$\rho_{S_p}(r) = \frac{1}{\pi^2}\int_0^\infty dp\, p^2 \frac{M^*(r)}{\sqrt{p^2+M^{*2}(r)}} \times \tag{2.29}$$

$$\times \frac{1}{\left(1 + e^{\beta\left(\sqrt{p^2+M^{*2}(r)}+g_\omega\omega(r)+g_\varrho\varrho(r)+eA(r)-\mu_p\right)}\right)},$$

$$\rho_{S_n}(r) = \frac{1}{\pi^2}\int_0^\infty dp\, p^2 \frac{M^*(r)}{\sqrt{p^2+M^{*2}(r)}} \times \tag{2.30}$$

$$\times \frac{1}{\left(1 + e^{\beta\left(\sqrt{p^2+M^{*2}(r)}+g_\omega\omega(r)-g_\varrho\varrho(r)-\mu_n\right)}\right)},$$

$$\rho_S(r) = \rho_{S_p}(r) + \rho_{S_n}(r), \tag{2.31}$$

$$\rho_B(r) = \rho_p(r) + \rho_n(r), \tag{2.32}$$

$$\rho_3(r) = \rho_p(r) - \rho_n(r). \tag{2.33}$$

Equations (2.23) to (2.33) constitute a highly nonlinear system for the nuclear densities, meson– and electromagnetic fields in RTTFA, which has to be solved selfconsistently. Of course the field equations (2.23) to (2.26) are the ones of the ground state case, the ground state densities replaced by integrals over Fermi distribution functions in (2.27) to (2.30). Nevertheless we considered it worthwhile to derive them again, starting with the Lagrangian (2.1) and therefore knowing at each step, what kind of approximation is made.

3 Thermostatic properties of hot nuclei

3.1 Subtraction mechanism

An isolated hot nucleus is a metastable system which tends to evaporate nucleons. To treat such a metastable nucleus within a static picture as an equilibrated hot nuclear system is reasonable only with a thermalization time smaller or at least comparable to any typical "decay"–time. In this case, the picture of a static nucleus embedded in its own evaporated nucleons may appear appropriate. In such an approach, the evaporated nucleons impose an artificial external pressure on the hot nucleus to compensate its tendency to decay. However, the remaining problem is how to isolate the properties of the hot nucleus from the contributions of the external nucleon vapor in a way that thermodynamical quantities, e.g. energy or entropy, do not depend on the size of the box in which the calculations are performed.

In the framework of nonrelativistic thermal Hartree-Fock calculations Bonche et.al. [12, 13] presented a way to treat the vapor separation problem by defining extensive quantities characterizing the nucleus as differences of these quantities for the nucleus+vapor and the vapor solutions they found. The idea of the method we used is based on earlier works by Myers [23] and Süßmann [24] concerning the desription of the nuclear surface by moments. Within nonrelativistic Thomas–Fermi calculations it has already been applied by Küpper [25].

Fig.1a) shows schematically a typical Thomas–Fermi density distribution at T>0. For radial distances larger than a certain radius R_β the system consists merely of the homogenous vapor phase β. We interpret the bulk region as a "liquid" phase α, which, for large enough nuclei, may also be homogenous for $r \leq R_\alpha$. The densities of the two homogenous phases α and β are ρ_α and ρ_β, respectively. To investigate the thermostatic properties of the finite system it is sufficient to look at the region $R_\alpha \leq r \leq R_\beta$, since they are in principle known for the homogenous phases α $(0 \leq r \leq R_\alpha)$ and β $(R_\beta \leq r < \infty)$ from nuclear matter calculations [6–11] (if there are no homogenous conditions in the bulk region of small nuclei, $R_\alpha = 0$). In this region $R_\alpha \leq r \leq R_\beta$ the transition between the "liquid" and the vapor phase takes place.

We start by defining a normalized density distribution

$$f(r) := \frac{\rho(r) - \rho_\beta}{\rho_\alpha - \rho_\beta} \tag{3.1.1}$$

and the corresponding surface distribution function

$$g(r) := -\frac{d\,f(r)}{d\,r}. \tag{3.1.2}$$

As pointed out in Refs. [23, 24] the properties of the nuclear surface can be described by moments of $g(r)$. Defining the "mth original surface moment"

$$[r^m] := \int_0^\infty dr\, r^m g(r), \tag{3.1.3}$$

the "equivalent sharp radius", for instance, is given by

$$R_S := \left[r^3\right]^{\frac{1}{3}}. \tag{3.1.4}$$

Thus by construction R_S is the radius of a uniform sharp distribution having the same volume integral as $f(r)$, i.e.,

$$\frac{4}{3}\pi\, R_S^3 = 4\pi \int_0^\infty dr\, r^2 f(r). \tag{3.1.5}$$

The functions $f(r), g(r)$ and the corresponding R_S are displayed in Fig.1b).

It turns out crucial that R_S is defined as an integral functional of the density distribution, not only containing "information" about one point of the continous $\rho(r)$ (as, for instance, the common half–value radius $R_{\frac{1}{2}}$).

Solving the RTTFA–equations (2.23) to (2.33) we used the "equivalent sharp radii" of the proton– and neutron density distributions to adjust the corresponding chemical potentials to the number of protons and neutrons, respectively:

$$Z = \frac{4}{3}\pi\, R_{S_p}^3\, \rho_{\alpha_p}, \tag{3.1.6}$$

$$N = \frac{4}{3}\pi\, R_{S_n}^3\, \rho_{\alpha_n}. \tag{3.1.7}$$

This corresponds to the picture of a system of two homogenous phases α and β with all the nucleus particles contained in the "liquid" phase α. It has to be stressed, that this physical picture is different from the one used in Refs. [12, 13, 15, 18]: our nucleus consists merely of the "liquid" phase inside the "equivalent sharp radii" embedded in its on vapor and with the phase transition taking place in the surface region. In contrast, Refs. [12, 13, 15, 18] are dealing with a nucleus consisting of both, a "liquid" and a vapor phase; i.e. a "liquid" nucleus put on a vapor layer. In such a picture, the phase transition takes place at any radial distance inside the nucleus when the vapor density is reached. In view of the motivating remarks at the beginning of this section, our approach seems more appropriate.

Once the densities and fields are determined selfconsistently, the thermodynamic quantities can be calculated in the usual manner. For the entropy one gets:

$$S = -\frac{\partial \Omega}{\partial T}\bigg|_{\mu,V} = \tag{3.1.8}$$

$$= -\frac{1}{\pi^2}\int_V d^3r \Big\{ \sum_{i=p,n} \int_0^\infty dp\, p^2 \Big[f_i(r,p)\ln f_i(r,p) + \big(1-f_i(r,p)\big)\ln\big(1-f_i(r,p)\big)\Big]\Big\},$$

with the Fermi distribution functions

$$f_i = \frac{1}{1+e^{\beta(\varepsilon_i-\mu_i)}}, \qquad i = p,n \tag{3.1.9}$$

and the one particle energies of protons and neutrons, respectively:

$$\varepsilon_p = \sqrt{p^2 + M^{*2}(r)} + g_\omega \omega(r) + g_\varrho \varrho(r) + eA(r), \tag{3.1.10}$$

$$\varepsilon_n = \sqrt{p^2 + M^{*2}(r)} + g_\omega \omega(r) - g_\varrho \varrho(r). \tag{3.1.11}$$

The energy of the system is given by:

$$E = \Omega + \mu_p Z + \mu_n N + TS =$$

$$= \int_V d^3r \Big\{ \frac{1}{2} g_\sigma \varphi(r)\rho_S(r) - \frac{1}{6} Mb\,(g_\sigma\varphi(r))^3 - \frac{1}{4} c\,(g_\sigma\varphi(r))^4 +$$

$$+ \frac{1}{2}\big(g_\omega\omega(r)\rho_B(r) + g_\varrho\varrho(r)\rho_3(r) + eA(r)\rho_p(r)\big) + \tag{3.1.12}$$

$$+ \frac{1}{\pi^2}\int_0^\infty dp\, p^2 \Big(\sqrt{p^2+M^{*2}(r)}\,\big(f_p(p,r)+f_n(p,r)\big)\Big)\Big\}.$$

However, expression (3.1.8) and (3.1.12) depend on the volume V of the box in which the calculations are performed. They are divergent with increasing V. To get convergent expressions we finally define, consistent with the definition of the "liquid" nucleus and first introduced by Küpper [25], the entropy and the energy of the isolated nucleus as:

$$S_A = \int_V d^3r(s(r) - s_\beta) + \frac{4}{3}\pi \left(R^3_{S_p} s_{\beta_p} + R^3_{S_n} s_{\beta_n}\right), \qquad (3.1.13)$$

$$E_A = \int_V d^3r(e(r) - e_\beta) + \frac{4}{3}\pi \left(R^3_{S_p} e_{\beta_p} + R^3_{S_n} e_{\beta_n}\right). \qquad (3.1.14)$$

s_{β_p} and s_{β_n} denote the proton– and neutron contributions to the entropy density of the vapor phase β, respectively. Analogue notations hold for the uniform energy density of β, $e_\beta = e_{\beta_p} + e_{\beta_n}$. For notational convenience we drop in the following sections the index A in equations (3.1.13) and (3.1.14) and refer in all expressions to the convergent quantities describing the hot nucleus without vapor.

3.2 Level density parameter

The nuclear level density [26] is of basic interest for statistical analysis of nuclear reactions as well as for nuclear astrophysics (see, for instance, Refs. [27, 28]). As it is well known, in an independent particle model and at "low" temperatures, the nuclear level density can be directly related to the level density parameter a by Bethe's formula [21]. In the same limit a can be expressed by the entropy or the single particle excitation energy:

$$S = 2aT, \quad E_X^{s.p.} = aT^2. \qquad (3.2.1)$$

We want to stress, that the *single particle* excitation energy is the natural input of Bethe's formula. Suraud et.al. [14] have shown within non-relativistic selfconsistent Thomas–Fermi calculations, that the range of validity of Bethe's formula and (3.2.1) can be extended with confidence up to T=4∼6 MeV, depending on the size of the nucleus under consideration. These relations do not hold for higher temperatures where the Fermi energy has faded due to the statistical occupation of continuum states. However,

one may *define* "effective" level density parameters [29]

$$a_E(T) = \frac{E_X(T)}{T^2}, \quad a_S(T) = \frac{S(T)}{2T}, \quad a_{SE}(T) = \frac{S^2(T)}{4E_X(T)}, \tag{3.2.2}$$

which coincide in the limit $T \to 0$ and $E_X \to E_X^{s.p.}$. E_X is the total excitation energy of the whole nucleus

$$E_X(T) = E(T) - E(0), \tag{3.2.3}$$

with the terms on the r.h.s. given by (3.1.12) for a given temperature and the total ground state energy, respectively. Thus the definition of E_X does not involve any density parameter by itself and contains, compared with the single particle excitation energy $E_X^{s.p.}$, which arises from phase space integrals over the one particle energies of equations (3.1.10) and (3.1.11) by an analogous definition, the meson contributions (see (3.1.12)). The replacement of $E_X^{s.p.}$ by E_X is motivated by the assumption, that E_X is a reasonable estimate of an experimental excitation energy $E_X^{exp.}$. Hence, the mayor point of a_E is the link it does establish between E_X and T in view of the experimental knowledge of these quantities.

Because a is approximately proportional to the mass number A=N+Z, one often writes it in the form $a = A/K$ and looks at the corresponding "effective" inverse level density parameters $K_i, i = E, S, SE$.

4 Results and discussion

4.1 Nuclear matter and the ground state of ^{208}Pb

For our calculations we have chosen a set of parameters from the literature [30], which fits accepted nuclear matter data. The coupling constants, masses and ground state nuclear matter properties are displayed in Table 1. The ϱ–meson coupling constant has been used to fit the experimental binding energy of ^{208}Pb within a Hartree calculation.

Symmetric nuclear matter calculations at finite temperatures have been performed by several authors (see, for instance, Refs. [6, 9]). At low temperature the theory possess a liquid-gas–phase transition. With a set of parameters reproducing ground state nuclear matter properties only slightly

different from the one we used, Jetter [6] found for normal nuclear matter density a critical temperature of $T_c \approx 17.2$ MeV.

In Table 2 we compare our Thomas–Fermi calculations for ^{208}Pb in its ground state with those of other authors and the corresponding Hartree results [30]. Concerning the comparison with the experimental value of the binding energy, center–of–mass corrections are not included in the theoretical calculations. The good agreement of the different Thomas–Fermi calculations may be seen as a test of the reliability of our code. The TFA results for the charge radius r_c are about 2% too large compared with the experiment. This is illustrated by Fig.2, where the corresponding charge density is compared with the experimental distribution represented by a so–called 3–parameter Fermi fit [31]. The bulk value of the charge density is too small within the semiclassical model, which also, as expected, cannot reproduce the quantal tail correctly.

The binding energy is overestimated by the TFA calculations while the Hartree approach yields an underbound nucleus. The relatively large discrepancy between Hartree– and TFA results is a consequence of the approximation made in the latter approach; i.e. the way the surface is described. Shell effects, which are of order 12 MeV for ^{208}Pb, cannot explain alone this discrepancy. As shown in Ref. [30], the TFA results depend also strongly on the set of parameters.

Refinements of the semiclassical description of ground–state nuclei by inclusion of quantum corrections are supposed to improve the results. Such investigations are performed at present by utilizing the extended relativistic Thomas–Fermi approximation at zero temperature (see Ref. [32]). However, at finite temperatures, as already mentioned in the introduction, the TFA approach becomes more and more reliable and should be sufficient for our present purposes.

4.2 Hot ^{208}Pb

The results presented in this section were obtained by solving the system of equations (2.23) to (2.33) followed by the calculation of the thermodynamic quantities of the hot nucleus as described in section 3. Problems occur due to the presence of the long–range Coulomb force. In this case, the vapor phase β is polarized by the long–range Coulomb field of the hot nucleus and the idea of a nuclear matter like vapor phase for large radial distances does

not hold anymore (Bonche et.al. [12, 13] found a solution of this problem in the framework of a nonrelativistic thermal Hartree–Fock model). For this reason we switched off the electromagnetic interaction in our calculations and looked at uncharged nuclei, as it is also done in Refs. [18, 25].

First of all, we checked the independence of our results on the size of the box in which the calculations were performed. Table 3 displays the energy E, entropy S, chemical potential μ and the "equivalent sharp radius" R_S of a hot uncharged isosymmetric nucleus with mass number A=160 for different radii R of the box at various temperatures (we will come back to such a system in the following section). S, μ and R_S are practically constant for all R while the changes in the energy E are of the order 1–2 MeV. This has to be seen in connection with the relativistic saturation mechanism, in which the small nuclear binding energy arises from the cancellation between the large scalar attraction and vector repulsion (see Table 5), which makes E very sensitive in relation to the numerical accuracy. However, the above "fluctuations" correspond to a maximal relative error of 0.3% and thus the results provide sufficient reliability.

In Table 4 we present our results for hot uncharged ^{208}Pb. It was shown in the framework of nonrelativistic semiclassical calculations [15] that the temperature does not noticeably affect the macroscopic static properties of nuclei up to T$\sim$4 MeV. Indeed we found the same kind of behaviour in our relativistic model, even extended to higher temperatures since the Coulomb field is unrealistically switched off. The variations of the chemical potentials between T=0 and T=5 MeV represent only about 10% of their variations over the whole temperature range under consideration. Concerning the "equivalent sharp radii" of the proton– and neutron density distributions, the temperature dependence in the low temperature region is even weaker and 10% of the total variation are reached at about T=7.5 MeV. This behaviour can also be seen in Fig.3 where we have plotted those quantities as a function of the temperature. Of course, the size of the system and hence the "equivalent sharp radii" increase with temperature while the decrease of the chemical potentials with increasing temperature can be understood in view of the standard Maxwell relations of the free energy [13]:

$$\left(\frac{\partial \mu_p}{\partial T}\right)_{V,Z,N} = -\left(\frac{\partial S}{\partial Z}\right)_{V,T,N}, \left(\frac{\partial \mu_n}{\partial T}\right)_{V,Z,N} = -\left(\frac{\partial S}{\partial N}\right)_{V,T,Z}. \qquad (4.2.1)$$

The results for the level density parameter in its three different versions

of equation (3.2.2) as a function of temperature are similar to those found in Ref. [13] by nonrelativistic Hartree–Fock calculations. There are only small variations of a few percent with the temperature. While the ratios show a tendency to decrease with increasing temperature up to T$\sim$12.5 MeV, an increasing behaviour can be observed for higher temperatures. As in Ref. [13], at any given temperature the three ratios are not equal, as would be expected from the relations (3.2.2). Though there are no significant deviations in the lower temperature region due to the lack of shell effects in our calculations, differences remain over the entire temperature range with the $S^2/4E_X$ ratio typically the largest and E_X/T^2 the smallest among the three. As already pointed out in Ref. [13] these deviations from the simplest Fermi gas relations are not surprising and it should be stressed again, that for higher temperatures they are defined as "effective" level density parameters (see section 3.2). We will come back to the level density parameter and a comparison of our results with experimental data in the following section.

In Fig.4 we present the proton– and neutron density distributions of uncharged ^{208}Pb at various temperatures. With increasing temperature the nucleus becomes less and less dense and the surface becomes more and more diffuse. At a temperature T$\sim$13.25 MeV we get a positive total energy (see Table 4). Within nuclear matter calculations this *limiting temperature* T_{lim} corresponds to the highest value of T for which the pressure can be negative as a function of the density; i.e for $T < T_{lim}$ self–cohesive nuclear systems may occur and so T_{lim} can be regarded as the maximum temperature for which the nucleus can exist. Our result for T_{lim} is in reasonable agreement with Ref. [33], where nuclear matter calculations were performed using an interaction which reproduces nuclear matter ground state properties only slightly different from the values we obtained (see Table 1) and a limiting temperature T_{lim}=13.009 MeV was found. Of course, our uncharged system is unrealistic and inclusion of the Coulomb repulsion will reduce T_{lim} significantly. It should also be mentioned, that T_{lim} depends strongly on the nuclear matter ground state incompressibility [13], which is determined by the chosen interaction. A lower value for K softens the equation of state which results for a given temperature $T < T_{lim}$ in a smoother dependence of the free energy on the density, which gives a less negative pressure. Thus a smaller incompressibility K yields a lower T_{lim}. Using a softer equation of state a limiting temperature of $T_{lim} \approx 12.5$ MeV was found in Ref. [13] for hot uncharged ^{208}Pb.

Further increase in temperature leads to systems with increasing positive total energy but which still show a surface. In the nuclear matter picture already mentioned above this corresponds to systems, where the pressure still has a maximum and minimum as a function of the density but cannot become negative anymore. The highest temperature at which we found such a solution is T=16.2 MeV. Above this value, we could find only solutions with uniform density distributions; the surface has completely disappeared, the maximum and minimum in the nuclear matter pressure curve coalesce into a point of inflexion. Indeed this behaviour is in reasonable agreement with the *critical temperature* $T_c \approx 17.2$ MeV found in the nuclear matter calculations of Ref. [6] within an only slightly different model. In the nonrelativistic case T_c=16.66 MeV was found [33].

Thus at temperatures in the range $T_{lim} \leq T \leq T_c$ we are confronted with the following situation: the artificial external pressure, which is imposed on the hot nucleus by its own evaporated nucleons is still large enough to create a surface though the total energy of the hot nucleus turned positive. Of course, such metastable states are not realistic in view of heavy ion collisions, where the whole picture of an external vapor pressure seems questionable, but they might be of interest for astrophysical applications. Looking at Fig.4 one tends to assume, that the creation of surfaces at $T_{lim} \leq T \leq T_c$ is a consequence of the finite size of the box; i.e. the homogenous vapor phase is not as well defined as it is at lower temperatures. Thus we performed calculations in that temperature range again, but in a significant larger box. The results confirmed our previous calculations: in the larger box the homogenous vapor phase is well defined and its pressure still creates surfaces.

In Table 5 we listed the kinetic energy and the partial contributions to the binding energy from the various mesons at different temperatures. As it is well known, there is a remarkably balanced cancellation between the contributions of the σ– and ω–meson (E_σ and E_ω, respectively). The term arising from the nonlinear σ–selfinteraction is important ($E_{\sigma_{NL}}$) and even the ϱ–meson contribution (E_ϱ) is not negligible for the heavy nucleus under consideration. The absolute values of all the meson contributions are decreasing with increasing temperature while the role of the kinetic energy becomes more and more important. At the limiting temperature $T = T_{lim}$ the kinetic energy exactly cancels the contributions provided by the mesons and at $T > T_{lim}$ the kinetic energy dominates. This behaviour can be further illustrated with Fig.5, where we have plotted the proton– (lower curves) and

neutron (upper curves) kinetic energy densities at the temperatures we also considered in Table 5. On the one hand the kinetic energy densities behave similar to the corresponding density distributions of Fig.4; i.e. their bulk values decrease and they are smoothing out with increasing temperature. On the other hand there is the temperature dependence of the "equivalent sharp radii" (see Fig.3), which are also indicated in Fig.5; i.e. the higher the temperature, the faster the "equivalent sharp radii" are growing with the temperature. Finally the latter effect becomes more and more important, the volume integrals over the distributions of Fig.5 grow faster and faster with increasing temperature and the system gets a positive total energy.

A conclusion arising from this section is the fact, that the properties of hot ^{208}Pb described within our relativistic model are very similar to the results obtained by various nonrelativistic approaches.

4.3 Temperature dependence of the level density parameter

During the last years strong attention has been devoted to the measurement of the level density parameter a for A$\approx$160 systems at excitation energies of 100 to 400 MeV [34–36]. It was found that a decreases from A/8 at low temperatures to A/13 at T$\approx$5 MeV. Stimulated by this observation a significant amount of theoretical work was done by several authors. It turned out, that the strong decrease of the level density cannot be explained with a pure mean field theory but by inclusion of correlations (collectivity). Such collective modes provide a significant contribution to the level density at low excitation energies, but largely disappear as the temperature is raised (see, for instance, Refs. [29, 37] and references therein). Though it is obvious that our relativistic mean field model is not able to reproduce this large decrease of a at temperatures T$\leq$4$\sim$5 MeV, we considered it worthwhile to compare our results with those recently published by de Lima Medeiros and Randrup [18], who used a nonrelativistic modified Seyler–Blanchard interaction which reproduces almost the same nuclear matter ground state properties as our model (see Table 1).

We performed calculations for an uncharged isosymmetric hot nucleus with mass number A=160. For determining the level density parameter $a_E(T)$ of equation (3.2.2) we used the excitation energy of the whole nucleus

$E_X(T)$. However, in view of the single particle excitation energy as the "natural" input of (3.2.2) (see section 3.2) we also calculated $E_X^{s.p.}(T)$ and found that the deviations from $E_X(T)$ are less than 6% over the whole range of temperature under consideration. Thus, from this point of view, the error made by the Fermi gas like definition in (3.2.2) is not large. The results for the inverse "effective" level density parameter K_E are shown in Fig.6 along with the values of Ref. [18] and experimental data. Before interpreting those results some remarks are necessary: for calculating the properties of hot nuclei in general and the temperature dependence of the level density parameter in particular, it is extremely important to treat the continuum states correctly. As a consequence, comparisons of models using different approaches to take the continuum states into account have to be done carefully. On the other hand, in the low temperature region such a special treatment or "subtraction procedure" is not "mandatory". This assumption was confirmed by the good agreement between nonrelativistic Hartree–Fock calculations with [12] and without [38] subtracting the continuum contributions for temperatures T$\leq$4$\sim$5 MeV. Within the corresponding semiclassical model the same trend was found [15]. Intuitively this can be illustrated by the density distributions for ^{208}Pb in Fig.4: looking at the proton (lower) curves, the uniform vapor density at large radial distances cannot be seen up to T=5 MeV within the resolution of our plots; the statistical occupation of states above the Fermi surface has been started but the excitation energy is small, so there is almost no vapor phase necessary to impose an artifical external pressure (see section 4.2). Thus the way, how this vapor phase is treated does not affect the results in the low temperature region significantly and we can compare our results with those of Ref. [18], in which the continuum contributions are treated in a different way. At temperatures up to T$\approx$6 MeV our results for K_E are roughly 7 to 12% smaller than those of Ref. [18]. This effect may be arises from the following: because of the leptodermous character of nuclei, $1/K$ can be expressed as a series in powers of $A^{-\frac{1}{3}}$ as it is done in Ref. [18] at zero temperature. In such an expansion, the term associated with the nuclear surface creates a quadratic dependence of the level density on the size of the system. As mentioned in section 4.1, the nuclear size of ^{208}Pb in its ground state is too large within our model, which could explain our smaller values for K_E compared to Ref. [18]. Another reason may be the spin–orbit interaction, which is included automatically in our relativistic model, but more quantitative investigations in this direction are necessary.

As mentioned above, both mean field models are not able to describe the high level density at T<4.5 MeV, but in the region 4.5 MeV$\leq$T$\leq$6 MeV our results are in good agreement with the available data. Inclusion of the Coulomb force will further decrease K_E and hence improve the agreement with the experiment, because the Coulomb contribution to the total energy decreases more slowly with increasing temperature than the other meson contributions which leads to higher excitation energies and a lower limiting temperature (see, for example, the results for charged and uncharged ^{208}Pb in Ref. [13]).

Compound nuclei at temperatures higher than T$\sim$5.5 MeV have not been detected. However, it is interesting to have a brief look at this temperature region which is unrealistic in relation to static models. When temperature increases the influence of the continuum states grows. The degeneracy of the Fermi gas is removed and the relation between E_X and T should shift from $E_X \propto T^2$ to its classical limit $E_X \propto T$; i.e the assumption of the Fermi gas expression of an infinite number of equidistant levels does not hold anymore; there is only a limited number of bound states available. Therefore there should be a decrease of the level density at higher temperatures relative to the values expected for a Fermi gas. This is the temperature region in which the subtraction procedure of the continuum contributions becomes more and more important because it is this subtraction which should "cancel" the Fermi gas like behaviour. Fig.6 shows, that our subtraction procedure cannot fulfil this demand; the relation $E_X \propto T^2$ remains "valid" over the whole temperature range. This is in agreement with the results of Ref. [13] (see Table 8 of that paper), where a similar subtraction mechanism has been used. On the other hand Fig.6 indicates, that the approach used by de Lima Medeiros and Randrup [18] is able to deliver a decreasing level density with increasing temperature. A similar behaviour was found by Dean and Mosel [39] who used again a different way to treat the continuum contributions. But we want to stress again, that in this high temperature region the physical picture of a hot static equilibrated nucleus becomes in general more and more unrealistic.

5 Concluding remarks

In the present work we have derived relativistic thermal Thomas–Fermi equations on the basis of a quantum hadrodynamical Lagrangian. Beside the coupling of σ–, ω– and ϱ–mesons to the nucleon field, nonlinear σ–selfinteractions and the electromagnetic field were taken into account. To treat the continuum contributions correctly, we presented a subtraction mechanism based on the "equivalent sharp radii" of the density distributions [23, 24].

For our calculations we have chosen a set of parameters from the literature [30] which fits accepted nuclear matter ground state data. We performed calculations for the ground state of ^{208}Pb and compared the results with Thomas–Fermi calculations of other authors, Hartree calculations and experimental data. The expected agreement between the different approximations and the experiment was recovered.

We then turned to the description of hot uncharged ^{208}Pb. First, we checked the independence of our results on the size of the box in which the calculations were performed and found them sufficiently reliable. By studying various thermostatic properties of the system we saw them not noticeably affected by the temperature up to T=5$\sim$7.5 MeV. At around T$\approx$13.25 MeV there exists a limiting temperature beyond which the total energy of the nucleus becomes positive. Further increase in temperature leads to systems which still possess a surface until the temperature reaches roughly the value of T_c from nuclear matter calculations. We investigated the various contributions to the binding energy, recovered the cancellation of the terms arising from the exchange of σ– and ω–mesons at different temperatures and found the expected growing importance of the kinetic energy with increasing temperature. In general our results are very similar to those of various nonrelativistic approaches.

Special attention was devoted to the level density parameter a. Therefore we performed calculations for a hot uncharged isosymmetric system with mass number A=160. Due to the lack of correlation effects our pure mean field model implies significantly smaller level densities than the experimentally extracted values at temperatures T<4.5 MeV. In the region 4.5 MeV$\leq$T$\leq$6 MeV our results are in good agreement with the available data and further improvement can be expected from the inclusion of the Coulomb field. For the high temperature region T>6 MeV we discussed the impact of the subtraction mechanism on the calculation of the level density

and compared the results of our model with different approaches by other authors. It turned out, that the subtraction procedure we used cannot provide an expected decrease of the level density at high temperatures, at which, on the other hand, the physical picture behind our model becomes in general more and more unrealistic.

Although many refinements could be included, especially the consideration of the Coulomb field for hot nuclei and of correlation effects, which are necessary to describe the level density at low temperatures, our approach constitutes a relatively simple quantum hadrodynamical frame, in which the behaviour of hot nuclei can be studied in a systematic way along with a tractable numerical effort.

Acknowledgements

One of us, D. Von-Eiff, would like to thank the Deutscher Akademischer Austauschdienst for a scholarship and to express his gratitude to the Nuclear Theory Group at the LBL for the kind hospitality. Useful discussions with W.D. Myers, W.J. Swiatecki and W. Stocker are gratefully acknowledged.

References

[1] B.D. Serot and J.D. Walecka, in "Advances in Nuclear Physics", Vol.16, ed. J.W. Negele and E. Vogt, Plenum Press, New York, London 1986

[2] J. Boguta and A.R. Bodmer, *Nucl. Phys.* **A292** (1977) 413

[3] Y.K. Gambhir et.al., *Ann. Phys. (N.Y.)* **198** (1990) 132

[4] M. Jetter et.al., *Europhys. Lett.* **14** (1991) 633

[5] F. Weber and M.K. Weigel, *Nucl. Phys.* **A493** (1989) 549

[6] M. Jetter, "Untersuchungen zur Anpassung der effektiven Kopplungskonstanten in der relativistischen Hartree– und Hartree–Fock–Theorie und deren Einfluß auf die Zustandsgleichung für Nukleonenmaterie", Diploma–Thesis, Ludwig–Maximilians–Universität Munich 1990

[7] B.M. Waldhauser et.al., *Phys. Rev.* **C36** (1987) 1019

[8] B.M. Waldhauser et.al., *Phys. Rev.* **C38** (1988) 1003

[9] N.K. Glendenning et.al., *Phys. Rev.* **C33** (1986) 1299

[10] N.K. Glendenning, *Nucl. Phys.* **A469** (1987) 600

[11] N.K. Glendenning, *Phys. Lett.* **B185** (1987) 275

[12] P. Bonche et.al., *Nucl. Phys.* **A427** (1984) 278

[13] P. Bonche et.al., *Nucl. Phys.* **A436** (1985) 265

[14] E. Suraud et.al., *Phys. Lett.* **B164** (1985) 212

[15] E. Suraud, *Nucl. Phys.* **A462** (1987) 109

[16] J. Schneider and W. Stocker, *Phys. Rev.* **A41** (1990) 5468

[17] D. Bandyopadhgay et.al., *Nucl. Phys.* **A511** (1990) 1

[18] E. de Lima Medeiros and J. Randrup, *Phys. Rev.* **C45** (1992) 372

[19] S. Song et.al., *Phys. Lett.* **B130** (1983) 14

[20] D. Von-Eiff and M.K. Weigel, *Z. Phys.* **A339** (1991) 63

[21] H.A. Bethe, *Rev. Mod. Phys.* **9** (1937) 53

[22] A.L. Fetter and J.D. Walecka, "Quantum Theory of Many–Particle Systems", McGraw–Hill, New York 1971

[23] W.D. Myers, *Nucl. Phys.* **A204** (1973) 465

[24] G. Süßmann, *Z. Physik* **A274** (1975) 145

[25] W.A. Küpper, "Thermostatische Eigenschaften von Kernen und semiinfiniter Kernmaterie im Thomas–Fermi–Modell", Ph.D. Thesis, Ludwig–Maximilians–Universität Munich 1978

[26] A.Bohr and B.R.Mottelson, "Nuclear Structure", Vol.1, Benjamin, New York 1969

[27] I.M. Govil et.al., *Phys. Lett.* **B197** (1987) 515

[28] T.J. Mazurek et.al., *Astrophys. J.* **229** (1979) 713

[29] S. Shlomo and J.B. Natowitz, *Phys. Lett.* **B252** (1990) 187

[30] M. Centelles et.al., *Nucl. Phys.* **A537** (1992) 486

[31] J. Heisenberg et.al., *Phys. Rev. Lett.* **23** (1969) 1402

[32] D. Von-Eiff, S. Haddad and M.K. Weigel, LBL–Preprint 31614, *Phys. Rev.* **C**, in press

[33] E. de Lima Medeiros and J. Randrup, *Nucl. Phys.* **A529** (1991) 115

[34] G. Nebbia et.al., *Phys. Lett.* **B176** (1986) 20

[35] K. Hagel et.al., *Nucl. Phys.* **A486** (1988) 429

[36] M. Gonin et.al., *Phys. Lett.* **B217** (1989) 406

[37] R.W. Hasse and P. Schuck, *Phys. Lett.* **B179** (1986) 313

[38] M. Brack and P. Quentin, *Phys. Scripta* **A10** (1974) 163

[39] D.R. Dean and U. Mosel, *Z. Phys.* **A322** (1985) 647

Table captions

table 1: Parameters and nuclear matter ground state properties (energy per particle E/A, particle density ρ_0, incompressibility K and effective mass M^*/M at saturation) of the set SRK3M7 [30].
$C_i^2 = g_i^2\ (M/m_i)^2\ , i = \sigma, \omega, \varrho$

table 2: Comparison of our TFA–results (TFAa) for the binding energy E and the charge radius r_c of ^{208}Pb in its ground state with those of other authors [30] (TFAb, Hartree; we used $r_c = \sqrt{r_p^2 + 0.8^2}$ fm) and experimental data [31].

table 3: Check of the independence of the subtracted quantities on the size R of the box for an uncharged isosymmetric nucleus with mass number A=160. μ and E are the chemical potential and the energy in MeV, respectively. R_S is the "equivalent sharp radius" in fm and S is the entropy.

table 4: Properties of hot uncharged ^{208}Pb.

table 5: Kinetic and potential energies coming from the exchange of σ–, ω– and ϱ–mesons and the nonlinear σ–meson selfinteraction ($E_{\sigma_{NL}}$) at different temperatures for uncharged ^{208}Pb. E is the total binding energy and E/A is the binding energy per particle. All quantities in MeV.

Table 1

M	=	939 MeV			
m_σ	=	500 MeV	C_σ^2	=	233.239
m_ω	=	783 MeV	C_ω^2	=	132.497
m_ϱ	=	763 MeV	C_ϱ^2	=	21.411
			$b \times 10^3$	=	3.292
			$c \times 10^3$	=	3.987

E/A	=	-16.0 MeV
ρ_0	=	$0.15\,\mathrm{fm}^{-3}$
K	=	300 MeV
M^*/M	=	0.75

Table 2

	E [MeV]	r_c [fm]
TFAa	-1698.8	5.53
TFAb	-1697.3	5.53
Hartree	-1620.1	5.50
Exp.	-1637.0	5.42

Table 3

T [MeV]		$R = 12.21$ fm	13.57 fm	14.92 fm
2	E	-2017.192	-2017.157	-2015.646
	S	45.522	45.522	45.522
	μ	-14.229	-14.229	-14.229
	R_S	6.235	6.235	6.235
6	E	-1647.697	-1648.184	-1648.192
	S	137.972	137.973	137.973
	μ	-16.311	-16.311	-16.311
	R_S	6.338	6.338	6.338
10	E	-930.624	-928.357	-928.965
	S	228.226	228.283	228.299
	μ	-20.284	-20.283	-20.283
	R_S	6.574	6.574	6.574

Table 4

T [MeV]	μ_p [MeV]	μ_n [MeV]	R_{S_p} [fm]	R_{S_n} [fm]	E [MeV]	S	E_X/T^2 [MeV^{-1}]	$S/2T$ [MeV^{-1}]	$S^2/4E_X$ [MeV^{-1}]
0.00	-24.03	-5.97	6.69	6.96	-2536.75	0.00			
2.50	-24.27	-6.50	6.70	6.99	-2441.93	74.90	15.17	14.98	14.79
5.00	-25.25	-7.87	6.77	7.06	-2166.70	148.54	14.80	14.85	14.91
7.50	-26.99	-9.96	6.90	7.17	-1710.13	221.62	14.70	14.77	14.85
10.00	-29.38	-12.77	7.09	7.36	-1080.85	294.37	14.56	14.72	14.88
12.50	-32.29	-16.30	7.40	7.65	-271.12	368.05	14.50	14.72	14.95
13.25	-33.25	-17.50	7.53	7.77	8.68	390.71	14.50	14.74	14.99
15.00	-35.63	-20.53	7.98	8.18	727.68	445.70	14.51	14.86	15.21
16.00	-37.09	-22.42	8.54	8.67	1194.22	482.47	14.57	15.08	15.60
16.20	-37.40	-22.82	8.77	8.87	1313.86	493.24	14.67	15.22	15.80

Table 5

	T=0.0	5.0	10.0	15.0
T_{kin}	3657.25	3816.81	4339.08	5216.24
E_σ	-20272.57	-19281.31	-16695.26	-12830.25
$E_{\sigma_{NL}}$	-1335.75	-1218.91	-907.72	-479.27
E_ω	15326.25	14433.78	12105.39	8756.25
E_ϱ	88.12	82.53	77.51	64.18
E	-2536.70	-2167.10	-1081.00	727.15
E/A	-12.20	-10.42	-5.20	3.50

Figure captions

figure 1: Schematic representation of the homogenous "liquid" ($0 \leq r \leq R_\alpha$) and vapor ($R_\beta \leq r < \infty$) phase (Fig.1a), the normalized density distribution $f(r)$, the corresponding surface distribution function $g(r)$ and the "equivalent sharp radius" R_S (Fig.1b).

figure 2: Charge density of ^{208}Pb at T=0 in TFA (dashed line) in comparison with a 3–parameter Fermi fit (solid line) to the experiment [31].

figure 3: "Equivalent sharp radii" of proton– (solid line) and neutron (dashed line) density distributions (Fig.3a) and chemical potentials of protons (solid line) and neutrons (dashed line) (Fig.3b) for uncharged ^{208}Pb as a function of temperature.

figure 4: Proton– (lower curves) and neutron (upper curves) density distributions for uncharged ^{208}Pb at various temperatures.

figure 5: Proton– (lower curves) and neutron (upper curves) kinetic energy densities in MeV·fm^{-3} as a function of the radial distance for uncharged ^{208}Pb at various temperatures. The "equivalent sharp radii" of the proton– and neutron density distributions are indicated.

figure 6: Inverse of the effective level density parameter $K_E = A/a_E$ in MeV as a function of the temperature for an uncharged isosymmetric nucleus with mass number A=160. The diamonds represent our calculated results, while the triangles are the results obtained in Ref. [18] by using a nonrelativistic modified Seyler–Blanchard interaction (the triangles are taken from Fig.3 of that paper). The solid curve is a fit to those results. The data points are taken from Fig.2 of Ref. [29].

Fig.1

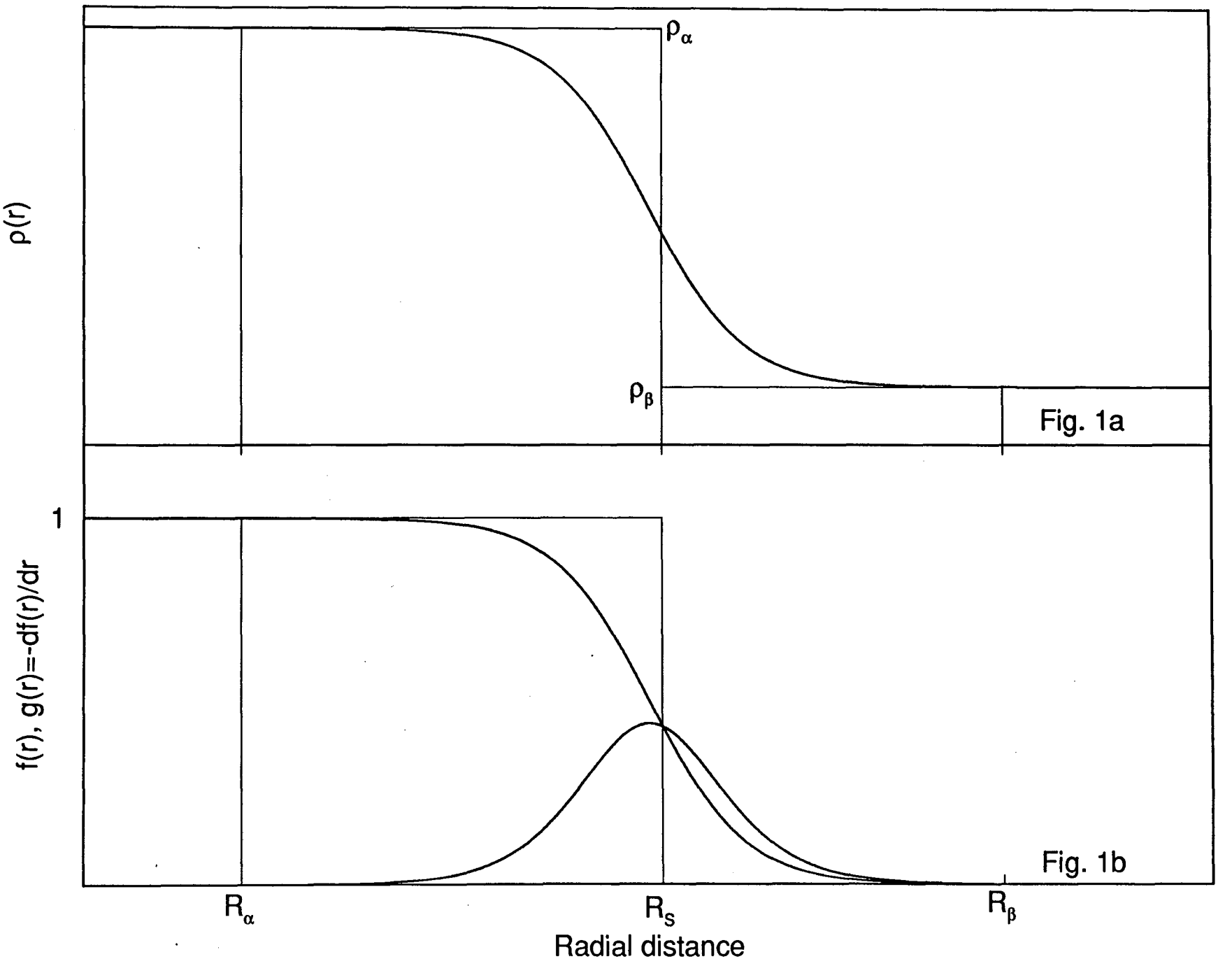

Fig.2

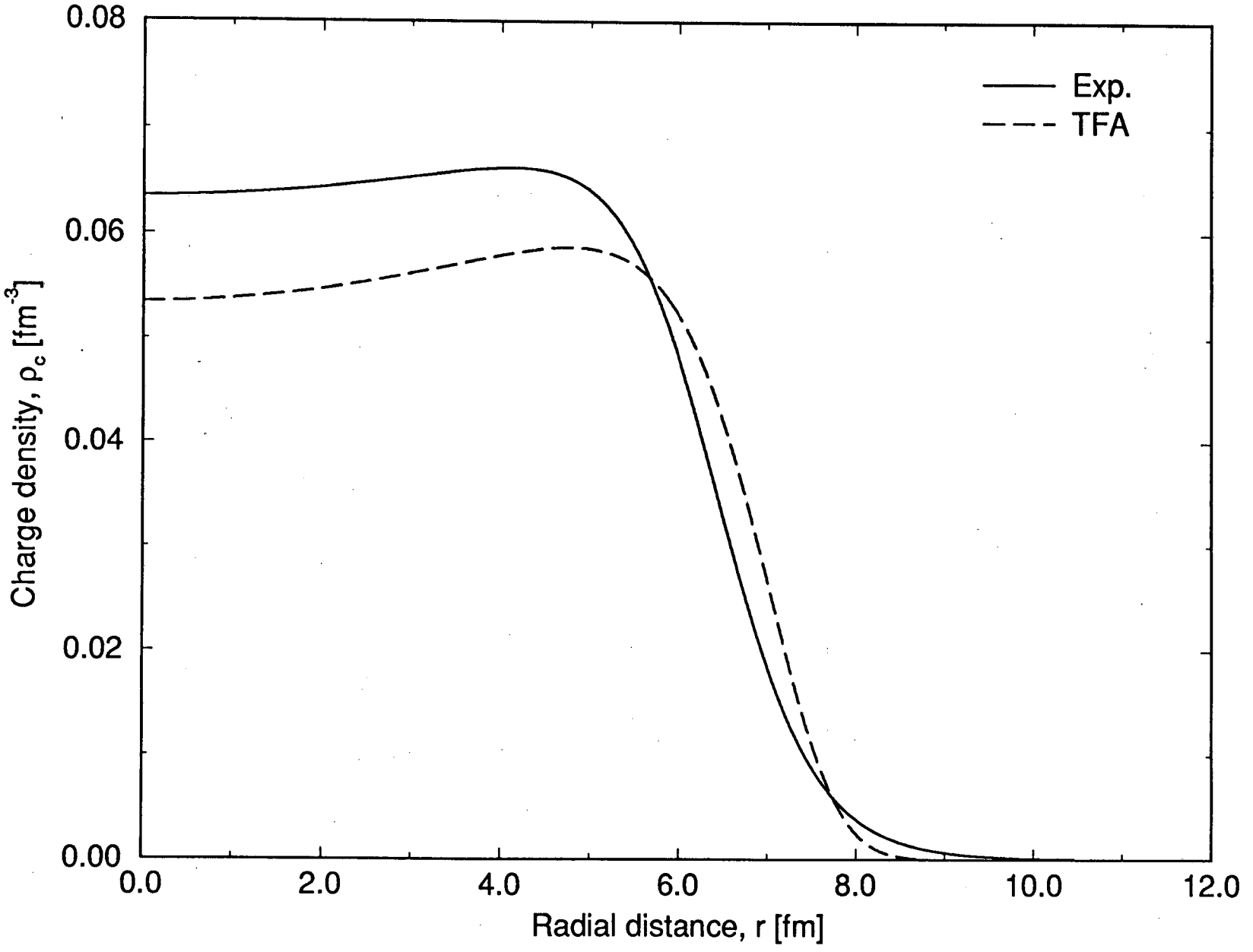
0.08
0.06
0.04
0.02
0.00
Charge density, ρ_c [fm^{-3}]
0.0
2.0
4.0
6.0
8.0
10.0
12.0
Radial distance, r [fm]
Exp.
TFA

Fig.3

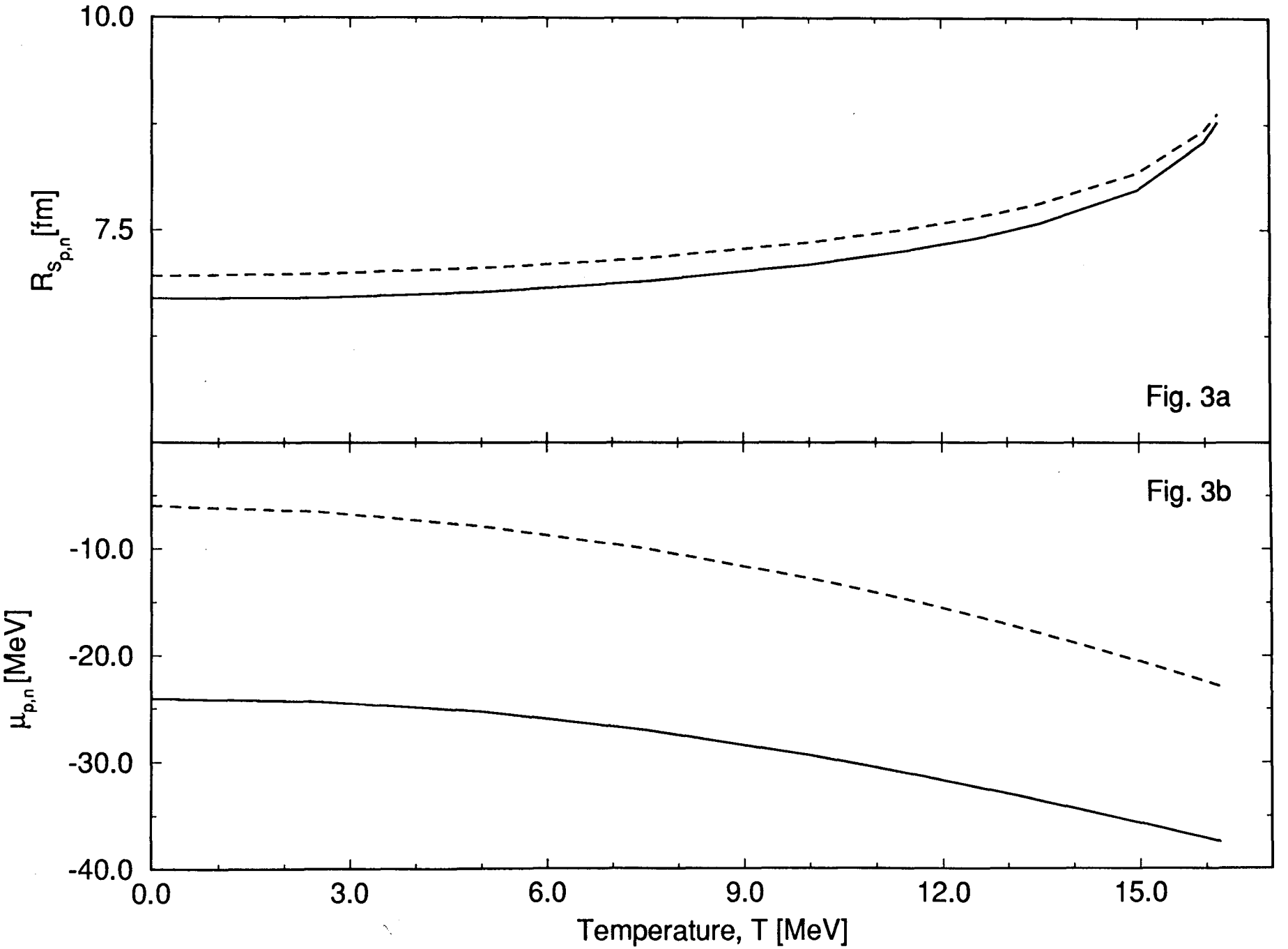
10.0
7.5
$R_{S_{p,n}}$ [fm]
Fig. 3a
Fig. 3b
-10.0
-20.0
-30.0
-40.0
$\mu_{p,n}$ [MeV]
0.0
3.0
6.0
9.0
12.0
15.0
Temperature, T [MeV]

Fig.4

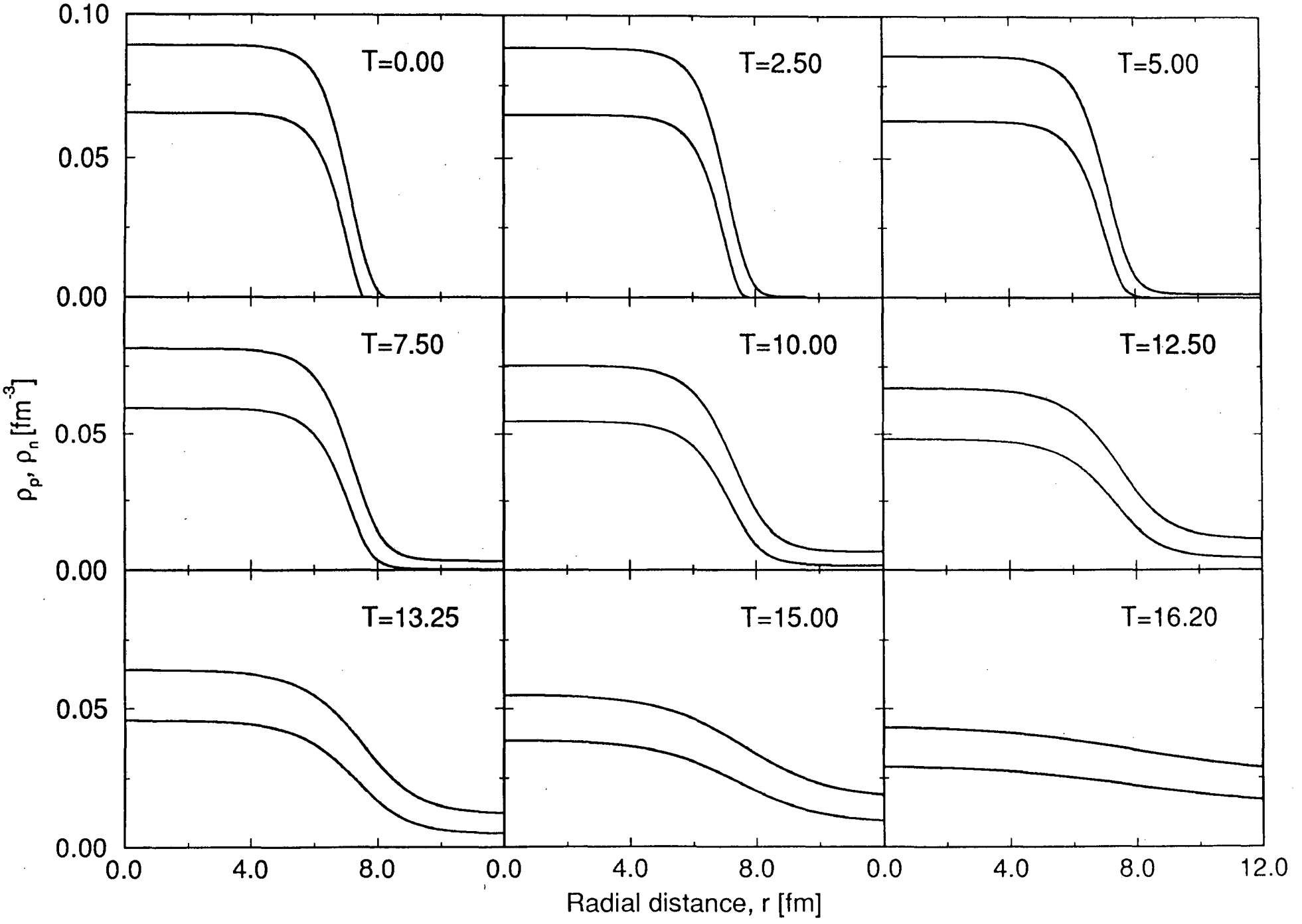
T=0.00
T=2.50
T=5.00
T=7.50
T=10.00
T=12.50
T=13.25
T=15.00
T=16.20
0.10
0.05
0.00
0.0
4.0
8.0
12.0
ρ_p, ρ_n [fm^{-3}]
Radial distance, r [fm]

Fig.5

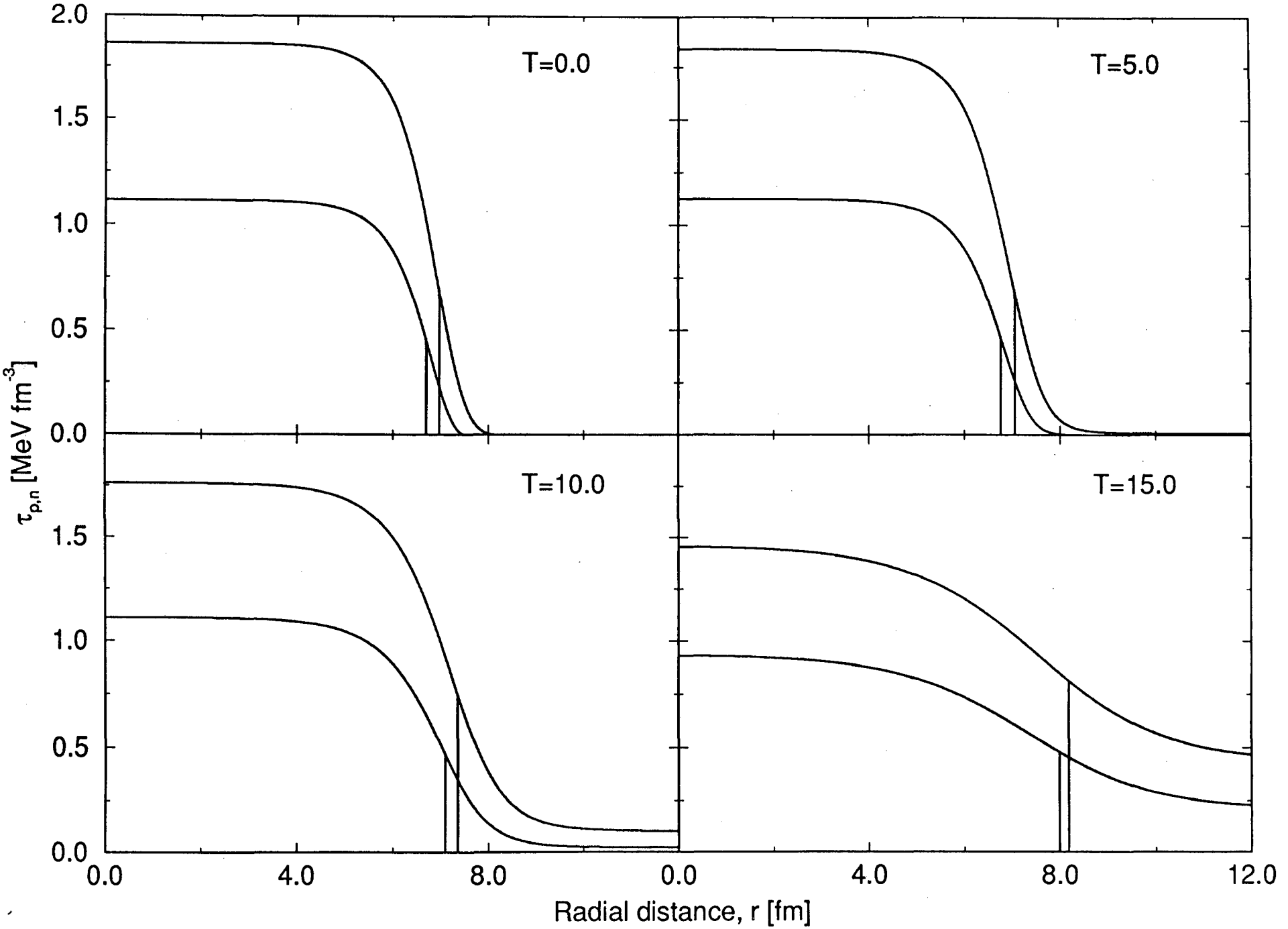
T=0.0
T=5.0
T=10.0
T=15.0
$\tau_{p,n}$ [MeV fm^{-3}]
Radial distance, r [fm]
0.0
0.5
1.0
1.5
2.0
4.0
8.0
12.0

Fig.6

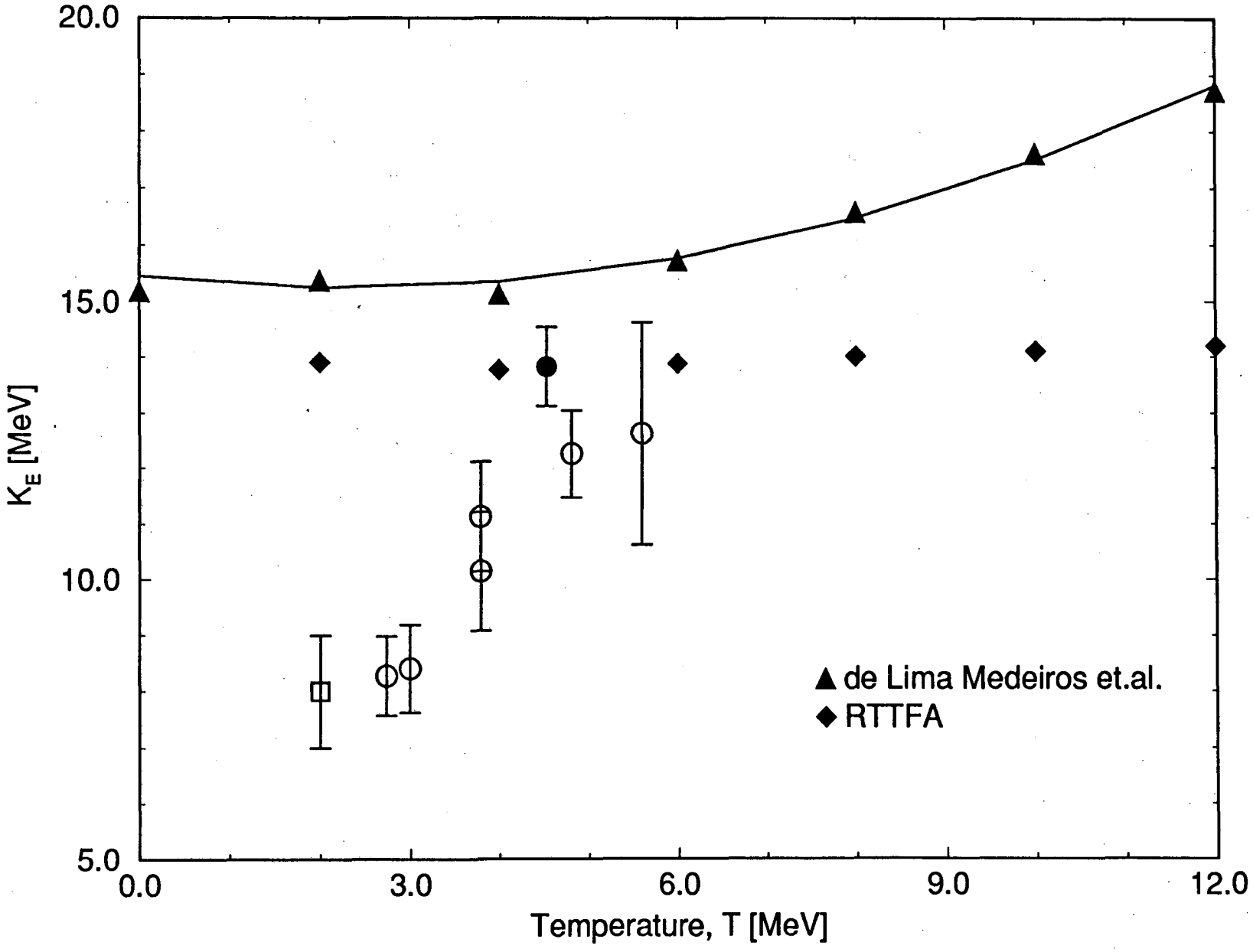
20.0
15.0
10.0
5.0
K_E [MeV]
0.0
3.0
6.0
9.0
12.0
Temperature, T [MeV]
de Lima Medeiros et.al.
RTTFA

LAWRENCE BERKELEY LABORATORY
UNIVERSITY OF CALIFORNIA
TECHNICAL INFORMATION DEPARTMENT
BERKELEY, CALIFORNIA 94720